

# Energy Level Alignment at Molecule-Metal Interfaces from an Optimally-Tuned Range-Separated Hybrid Functional

Zhen-Fei Liu,<sup>1,2, a)</sup> David A. Egger,<sup>3, a)</sup> Sivan Refaely-Abramson,<sup>3</sup> Leeor Kronik,<sup>3, b)</sup> and Jeffrey B. Neaton<sup>1,2,4, c)</sup>

<sup>1)</sup>*Molecular Foundry and Materials Sciences Division, Lawrence Berkeley National Laboratory, Berkeley, California 94720, USA*

<sup>2)</sup>*Department of Physics, University of California, Berkeley, California 94720, USA*

<sup>3)</sup>*Department of Materials and Interfaces, Weizmann Institute of Science, Rehovoth 76100, Israel*

<sup>4)</sup>*Kavli Energy Nanosciences Institute at Berkeley, Berkeley, California 94720, USA*

(Dated: 7 March 2017)

The alignment of the frontier orbital energies of an adsorbed molecule with the substrate Fermi level at metal-organic interfaces is a fundamental observable of significant practical importance in nanoscience and beyond. Typical density functional theory calculations, especially those using local and semi-local functionals, often underestimate level alignment leading to inaccurate electronic structure and charge transport properties. In this work, we develop a new fully self-consistent predictive scheme to accurately compute level alignment at certain classes of complex heterogeneous molecule-metal interfaces based on optimally-tuned range-separated hybrid functionals. Starting from a highly accurate description of the gas-phase electronic structure, our method by construction captures important nonlocal surface polarization effects via tuning of the long-range screened exchange in a range-separated hybrid in a non-empirical and system-specific manner. We implement this functional in a plane-wave code and apply it to several physisorbed and chemisorbed molecule-metal interface systems. Our results are in quantitative agreement with experiments, both the level alignment and work function changes. Our approach constitutes a new practical scheme for accurate and efficient calculations of the electronic structure of molecule-metal interfaces.

## I. INTRODUCTION

Interfaces between molecules and metals play a central role in emerging functional devices in nanoscience and nanotechnology<sup>1–10</sup>. When a molecule is adsorbed on a metal surface, several important physical and chemical phenomena occur. For example, an interface dipole forms, altering the work function of the metal surface<sup>1,11</sup>; discrete molecular frontier orbitals hybridize with extended metallic states, forming molecular resonances; and substrate screening effects shift orbital energies. A key physical observable is the energy level alignment between the frontier molecular resonance peak positions and the Fermi level,  $E_F$ , of the metal; this alignment can be directly linked to the energy barrier and efficiency of charge transfer across the interface. For example, in molecular junctions, highest occupied molecular orbital (HOMO) or the lowest unoccupied molecular orbital (LUMO) resonance energies relative to  $E_F$  are central to determining the zero-bias conductance of the junction, as shown in Ref. 12. Molecule-metal bonding spans a range of binding energies and degrees of hybridization strengths<sup>6,8,9</sup>, from weak physisorption to strong chemisorption; in many cases where covalent or molecule-metal interactions associated with significant

charge transfer occur, molecular signatures in the interface electronic structure are nonetheless observed. For these intermediate cases, molecular resonances can be energetically close to or at the metal Fermi level, which is generally an indication of strong charge transfer between the two systems<sup>13</sup> and of significant and complex changes to the interface dipole. Because level alignment and charge transport are intertwined, its accurate description is of general importance for understanding, controlling, and predicting functional properties at a variety of interfaces, including systems related to energy conversion and storage.

Experimentally, energy level alignment can be determined by direct photoemission spectroscopy for occupied molecular orbitals, and by inverse photoemission spectroscopy for unoccupied molecular orbitals.<sup>1,4–6</sup> Conductance measurements<sup>14–16</sup> of molecular junctions probe charge transport properties and, thus, include indirect information about the level alignment. However, in principle, distinct binding geometries of molecules in junctions can lead to different level alignment<sup>17</sup> and, hence, charge transport properties<sup>18</sup>, and as charge transport measurements are usually ensemble averages of multiple geometries, care must be taken in relating conductance to level alignment in such measurements<sup>12,18,19</sup>.

First-principles electronic structure calculations that can model individual, well-defined geometries provide additional information complementary to experiments. From a formal theory viewpoint, molecular levels at interfaces are quasiparticle energy levels, i.e., they correspond to charged excitations. A rigorous formalism for

<sup>a)</sup>These authors contributed equally.

<sup>b)</sup>Electronic mail: leeor.kronik@weizmann.ac.il

<sup>c)</sup>Electronic mail: jbeaton@lbl.gov

quasiparticle energies is many-body perturbation theory (MBPT), which in practice is most often used in the  $GW$  approximation<sup>20,21</sup>, where  $G$  is the single-particle Green’s function and  $W$  is the screened Coulomb interaction.  $GW$  has been shown to be an accurate approach for a wide range of molecules<sup>22–27</sup> and bulk solids<sup>28–30</sup>. However, several issues have hindered the widespread use of  $GW$  calculations for molecule-metal interfaces. Firstly, due to its high computational cost, even with today’s computing power it is still far challenging to perform  $GW$  calculations of several hundred atoms with periodic boundary conditions, as is the case for molecule-metal interfaces<sup>31–34</sup>. Moreover, several benchmarking studies, including work on smaller molecule-metal systems, also showed that results from perturbative  $GW$  calculations can be challenging and expensive to converge numerically<sup>23,35,36</sup>. Furthermore, it is by now well-known that single-shot  $GW$  calculations often depend on the underlying starting point,<sup>22,37,38</sup> which adds additional complications for efficient  $GW$  calculations of large-scale molecule-metal interfaces and their functional properties.

Balancing accuracy and efficiency is crucial for calculations of molecule-metal interfaces, and density functional theory (DFT)<sup>39,40</sup> is usually the pragmatic choice for first-principles calculations at relatively moderate computational cost, provided it is accurate enough. Formally, however, eigenvalues of Kohn-Sham (KS) Hamiltonians are only zeroth order approximations to quasiparticle energies<sup>41</sup>. In fact, there is no theorem guaranteeing that they are quantitatively accurate, with the important exception of the HOMO energy, for which the ionization potential (IP) theorem holds<sup>42–44</sup>. For the band gap of a semiconductor (or, equivalently, the molecular HOMO-LUMO gap), even the exact functional in KS DFT is not necessarily accurate, as it lacks a derivative discontinuity<sup>45</sup> in the exchange-correlation (XC) potential owing to its strictly local, multiplicative nature<sup>46–48</sup>.

Fig. 1 schematically shows representative energy levels for the molecule-metal interface. The right hand side illustrates the situation for an isolated gas-phase molecule, for which there is a well-defined quasihole level denoted as HOMO, which is equal to the negative of the IP, and a well-defined quasielectron level denoted as LUMO, which is equal to the negative of the electron affinity (EA). For the molecule adsorbed on the metal surface, in Fig. 1 we denote resonances that appear as peaks in the projected density of states (PDOS) - where the DOS has been projected onto the molecular subspace - as HOMO and LUMO, which are now broadened due to hybridization. Comparing the molecular energy levels of the gas phase and the adsorbed molecule, Fig. 1 illustrates the important physical phenomenon of surface-induced gap renormalization<sup>49–52</sup>: when the molecule is close to the surface, electrons in the metal respond to and screen single-particle excitations in the molecule, i.e., free carriers in the metal polarize when a hole/electron is added to the molecule and screen the Coulomb interactions in the molecule. As a result, when the molecule approaches

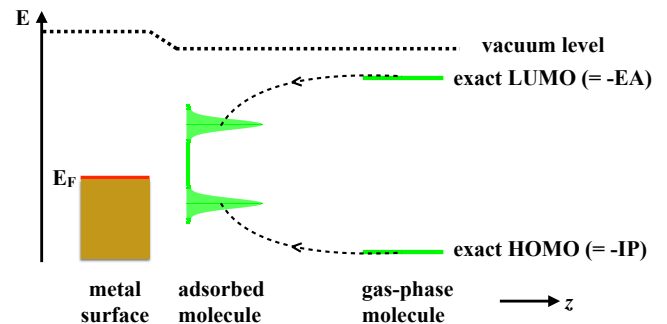


FIG. 1. Relevant energy levels at a molecule-metal interface. Green lines (shaded areas) represent exact quasiparticle levels (PDOS of the adsorbed molecule). Note that for the case of the adsorbed molecule, broadened molecular resonances are shown. Dashed arrows indicate the surface-induced renormalization of the molecular levels, which depends on the molecule-metal distance,  $z$ . The sign of the vacuum level change at the interface, a result of the interface dipole, is taken here to be negative. For easy visualization, we align the interface-modified vacuum level with that of the gas-phase molecule.

the surface, the HOMO and LUMO energies move closer to  $E_F$  and the HOMO-LUMO gap is reduced.<sup>49–52</sup> For weakly coupled physisorbed molecules, the energy change of the molecular levels relative to  $E_F$  as a function of the molecule-metal distance has been shown to follow a classical image-like form<sup>50</sup>, and renormalization is sometimes referred to as an “image-charge effect”. The effective “image potential” is given by  $1/[4(z - z_0)]$ , where  $z$  is the average height of the molecule on the surface and  $z_0$  is the image plane position. It is an effective one-body potential resulting from a many-body effect, namely non-local correlation, rather than from a static perturbation to the system. Fig. 1 also shows how the vacuum levels are aligned at the interface and for the gas-phase molecule. The vacuum level can increase or decrease at the interface (only one case is shown in Fig. 1), due to formation of the interface dipole.

Results from calculations using the local density approximation (LDA)<sup>40</sup> and typical generalized gradient approximations (GGAs) in the Kohn-Sham (KS) DFT scheme, while often accurate for total energy or charge density related properties of molecule-metal interfaces such as work-function changes<sup>53–59</sup>, typically strongly underestimate the band gap of molecules and semiconductors<sup>21</sup>. We illustrate this with grey dashed lines in Fig. 2, namely that LDA/GGA misplace the HOMO and LUMO levels in the gas phase, such that the gap is underestimated. Moreover, in typical LDA/GGA calculations of molecule-metal interfaces, one finds that the HOMO-LUMO gap for the adsorbed molecule remains virtually the same as in the gas phase. In other words, LDA and GGA results for the level alignment are not sensitive to changes in screening environment and fail

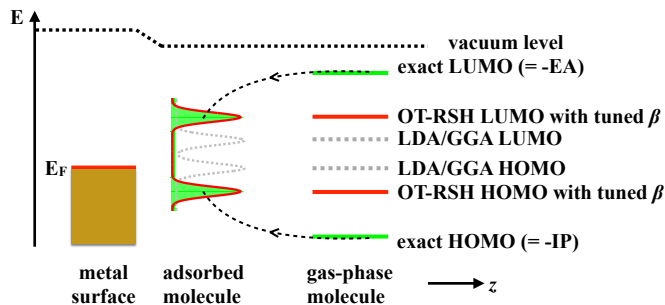


FIG. 2. Energy levels at a molecule-metal interface. Green lines represent exact quasiparticle levels, grey dashed lines approximate LDA/GGA levels, and red lines OT-RSH levels as computed with the method introduced in this paper (see text for details). Note that for the case of the adsorbed molecule, broadened molecular resonances are shown. Dashed arrows indicate the surface-induced renormalization of the molecular levels, which depends on the molecule-metal distance,  $z$ . The sign of the vacuum level change at the interface, a result of the interface dipole, is taken here to be negative. For easy visualization, we align the interface-modified vacuum level with that of the gas-phase molecule.

to capture the gap renormalization effect. This is because LDA and GGAs consist of local correlation only whereas renormalization is a nonlocal effect<sup>49–52</sup>. As we discuss below, similar findings hold for conventional global and screened hybrid functionals.

The high computational cost and convergence challenges associated with *GW*, together with the formal and practical issues of popular XC functionals in predicting level alignments, led to the development of several correction schemes following various directions, see Refs. 50,51,57,60–69 for examples. Specifically for physisorbed systems, one can assume weak coupling between the molecule and the metal, and attempt to shift the PDOS peaks in a non-self-consistent, adjustable-parameter-free *a posteriori* manner. One example for such a non-self-consistent correction scheme is the DFT+ $\Sigma$  approach<sup>50</sup>, where  $\Sigma$  denotes a two-step correction to KS eigenvalues: (1) it uses a gas-phase correction, equal to the difference between the gas-phase LDA/GGA HOMO or LUMO energy and a value obtained from a more accurate approach (e.g., *GW*) that is closer to the exact quasiparticle energy (cf. Figs. 1 and 2); and (2) a correction accounting for the surface polarization responsible for gap renormalization, which is often approximated using a classical image-charge model<sup>50</sup>,  $1/[4(z - z_0)]$ , where  $z$  is the average distance between the adsorbed molecule and the surface, and  $z_0$  is the image-plane position. We note that recently we have augmented this approach by using a non-classical DFT-determined image plane of the metallic surface to compute the surface polarization term, rather than the classical DFT-derived image plane<sup>70</sup>. The DFT+ $\Sigma$  method has been used to successfully predict and explain level alignment at physisorbed

interfaces<sup>70</sup> and charge transport in specific molecular junctions where the above-mentioned weak-coupling assumption is reasonable<sup>12</sup>.

Of major interest are approximate *GW*-inspired theoretical approaches that can go beyond the weak-coupling assumption to also treat molecules chemisorbed on metals, i.e., when a significant amount of charge is transferred between the two subsystems. Examples include systems for which molecular levels are pinned at  $E_F$ <sup>71,72</sup>, or where significant covalent interactions lead to strong hybridization between molecular and substrate orbitals<sup>73</sup>, such as the Au-benzenedithiol-Au junction<sup>74,75</sup>. As mentioned above, this situation can lead to the molecular resonances being energetically close to the Fermi level, which implies a significant charge transfer. Clearly, the amount of charge transfer will determine the distribution of the charge density of the interface system, which means that a correction scheme for level alignment requires self-consistency. This notion also implies that in case of chemisorption an incorrect description of level alignment can yield errors in the density and, at least in principle, result in incorrect interface dipoles,<sup>57</sup> work functions, and total energies of molecule-metal systems. Therefore, we currently seek a theoretical method that can accurately and efficiently characterize the interface electronic structure in a self-consistent manner, and thus is applicable to physisorbed and, in particular, also to more strongly bound and partially chemisorbed molecule-metal systems. With such an approach in hand, one is able to improve the prediction of relevant interface properties beyond level alignment, including work function changes and PDOS lineshapes.

Here, we present a new method aiming in the vein of reliable and self-consistent determination of the level alignment at molecule-metal interfaces. Our conceptual framework is the generalized Kohn-Sham (GKS) scheme<sup>76</sup>, which is still a DFT approach but in contrast to LDA/GGA builds on an effective potential that is nonlocal. Hybrid functionals, in which (semi)local functionals are mixed with a fraction of Fock exchange, are a special case of GKS DFT. Popular hybrid functionals were shown to greatly improve GGA results for both total energy related properties, such as thermochemistry<sup>77</sup>, as well as quasiparticle energy levels, such as band gaps<sup>78</sup>. However, conventional hybrid functionals do not in general remedy the energy level alignment problem at interfaces<sup>70,79</sup>. Notably, conventional hybrids cannot capture the renormalization of the HOMO-LUMO gap. A relatively recent and particularly promising class are optimally-tuned range-separated hybrid (OT-RSH) functionals<sup>43,80</sup>, in which parameters of the functional are tuned per system to satisfy important physical conditions, without recourse to empirical data or any fitting. OT-RSH was shown to yield accurate frontier orbital energy levels, outer-valence electron spectra, and HOMO-LUMO gaps of gas-phase molecules<sup>81–89</sup> and molecular crystals<sup>90,91</sup>, as well as transport properties<sup>92,93</sup>. In this work, we extend the applicability of this functional to

heterogeneous molecule-metal interfaces by proposing a route for a judicious choice of optimal parameters in the OT-RSH functional. This yields a fully self-consistent OT-RSH scheme which is applicable to both physisorbed and chemisorbed molecule-metal systems and thus extends methods reliant on the weak coupling limit. Using it for several prototypical test cases, we achieve quantitative agreement with experiments for level alignment and work function changes including those featuring charge transfer and stronger bonding.

The outline of this paper is as follows: In Sec. II, we briefly review the OT-RSH functional as applied to gas-phase molecules and molecular crystals, and then present our approach for treating molecule-metal interfaces. In Sec. III, we apply the method to six molecule-metal interfaces that have been well-studied in both theory and experiment, including two systems where charge transfer and Fermi level pinning occur. In Sec. IV, we discuss limitations of the proposed method and outline remaining challenges, which is followed by our conclusions in Sec. V.

## II. METHODOLOGY

### A. OT-RSH for gas-phase molecules and molecular crystals

In RSH functionals, the Coulomb operator is decomposed into short-range and long-range components<sup>94</sup>. In this approach, proposed by Yanai et al.<sup>95</sup>, the decomposition takes the form

$$\frac{1}{|\mathbf{r} - \mathbf{r}'|} = \frac{\alpha + \beta \text{erf}(\gamma |\mathbf{r} - \mathbf{r}'|)}{|\mathbf{r} - \mathbf{r}'|} + \frac{1 - [\alpha + \beta \text{erf}(\gamma |\mathbf{r} - \mathbf{r}'|)]}{|\mathbf{r} - \mathbf{r}'|}, \quad (1)$$

where  $\alpha$ ,  $\beta$ , and  $\gamma$  are parameters and  $\text{erf}(\cdot)$  is the error function. We note that this partition is not unique, but the choice of the error function is computationally convenient. Here, we treat the first term using nonlocal Fock exchange and the second using semi-local exchange. The exchange-correlation energy can then be written as

$$E_{XC} = \alpha E_{X,SR}^{\text{EXX}} + (1 - \alpha) E_{X,SR}^{\text{GGA}} + (\alpha + \beta) E_{X,LR}^{\text{EXX}} + (1 - \alpha - \beta) E_{X,LR}^{\text{GGA}} + E_C^{\text{GGA}}, \quad (2)$$

where the subscript X (C) denotes exchange (correlation), SR (LR) denotes the short-range (long-range) exchange, and the superscript EXX (GGA) reflects whether the corresponding energy component is treated using Fock exchange (GGA exchange or correlation). In this work, we follow Ref. 84 and use PBE (Perdew-Burke-Ernzerhof)<sup>96</sup> for the GGA exchange ( $\omega$ PBE<sup>97</sup> for the SR part) and correlation components.

For an isolated gas-phase molecule,  $\alpha$  is often chosen to be 0.2,<sup>84,85,98</sup> and then  $\beta$  is chosen as  $1 - \alpha = 0.8$  to ensure

the correct asymptotic potential<sup>42</sup> via enforcing full long-range Fock exchange. Here, we will use the notation  $\beta_0 = 0.8$  to denote the  $\beta$  value appropriate for isolated gas-phase molecules.  $\gamma$  is the range-separation parameter and governs the separation between SR and LR. In the OT-RSH approach,<sup>43,80,81</sup> the remaining parameter  $\gamma$  is tuned separately for each system by minimizing

$$J(\gamma) = |\varepsilon^\gamma(N) + \text{IP}^\gamma(N)|^2 + |\varepsilon^\gamma(N+1) + \text{IP}^\gamma(N+1)|^2, \quad (3)$$

where  $\varepsilon$  are GKS HOMO eigenvalues, the IP is calculated using total energy differences between neutral and charged systems, and  $N$  ( $N+1$ ) indicates the neutral molecule (anion).

Ref. 90 generalized the OT-RSH functional to the case of molecular crystals.  $\alpha$  and  $\gamma$  were chosen according to the gas-phase values, but  $\beta$  was adapted to account for changes in the long-range Coulomb screening due to the presence of the other molecules in the crystal and the difference in dielectric environment compared to an isolated molecule. From Eq. (2), we see that  $\alpha + \beta$  governs the fraction of long-range Fock exchange. For a molecular crystal with an average dielectric constant  $\epsilon$ , Ref. 90 proposed to use  $\alpha + \beta = 1/\epsilon < 1$ . This choice of  $\beta$  was shown to correctly describe the gap renormalization in molecular crystals compared to a single gas-phase molecule and optical absorption<sup>99</sup>.

### B. OT-RSH for molecule-metal interfaces

We first note that for a fixed,  $z$ -independent choice of  $\alpha$ ,  $\beta$ , and  $\gamma$ , the OT-RSH functional *cannot* capture the  $1/[4(z - z_0)]$  behavior of the image-charge effect and gap renormalization of the adsorbate in the weak-coupling physisorbed limit at a metal surface for all  $z$ . To understand why, consider that in Ref. 50, it was shown that the physical origin of the gap renormalization is the change in the screened Coulomb interaction,  $\Delta W$ , between the isolated molecule and the adsorbate. From a GKS viewpoint, this long-range correlation effect would require a *change* in the amount of long-range screened Fock exchange as a function of molecule-metal distance, which Eq. (2) with fixed parameters lacks. In fact, this is also the case for any standard local, semi-local, or hybrid functional, as was shown in Ref. 79 using the PBE and HSE (Heyd-Scuseria-Ernzerhof)<sup>100</sup> functionals as examples.

As described above, in Ref. 90,  $\beta$  was tuned from  $\beta_0$  to  $1/\epsilon - \alpha$  in order to capture the change in Coulomb screening between an isolated molecule and a molecular crystal. Inspired by this idea, and given the fact that the image-charge effect is a long-range effect, we propose to account for the change in long-range Fock exchange at a molecule-metal interface by insisting on  $\alpha + \beta < 1$  for the interface and tuning  $\beta$  so as to capture the renormalization of the orbital resonance energies at the level of an image-charge model. For  $\alpha$  and  $\gamma$ , it is clear that in



the limit of very weak physisorption the optimal value obtained in the gas phase is maintained on the surface as the molecular density remains unchanged. For chemisorbed systems with exchange of charge between molecule and metal, of course this does not hold anymore, but as we show below the optimal value for  $\gamma$  is virtually unaffected by small charge density rearrangements. Thus, for each molecule-metal system we choose  $\alpha = 0.2$  and  $\gamma$  based on Eq. (3) as obtained for the gas-phase molecule. The problem left is how to choose the optimal  $\beta$  for the interface such that the renormalization induced by the surface is accounted for (see red lines of Fig. 2). Here, we choose  $\beta$  such that the orbital energies renormalize properly according to  $1/[4(z - z_0)]$ . To avoid a complicated functional form with explicit treatment of this effect, we here use a DFT-based image-charge model: it allows for determining a non-classical image-plane position for each type of surface in a unique way<sup>70</sup>, from which we determine the amount of orbital renormalization. If we keep  $\beta$  as a simple scalar parameter, it should implicitly depend on  $z$  due to the  $z$ -dependence in the image-charge model. Furthermore, we make the assumption that the orbital energies of the isolated molecule and the PDOS peaks of the adsorbate change by the same amount when  $\beta$  is varied from  $\beta_0$  to  $\beta < 1 - \alpha$ , while keeping  $\alpha$  and  $\gamma$  at their gas-phase values. Therefore we can tune  $\beta$  in the gas phase, which reduces the computational cost, and choose  $\beta$  such that the neutral gas-phase HOMO changes by an amount equivalent to the image-charge energy, such that

$$\varepsilon_N^\gamma(\beta) - \varepsilon_N^\gamma(\beta_0) = P, \quad (4)$$

where subscript  $N$  denotes the neutral gas-phase system and  $P = 1/[4(z - z_0)]$  is the image-charge energy determined as in Ref. 70. We note that the substrate provides significant screening, and the  $\beta$  defined in this way can become negative. Considering that  $\beta = -\alpha$  corresponds to the limit of fully screened LR Fock exchange, we choose this value as our lower limit (i.e.,  $\beta \geq -0.2$  when  $\alpha$  is chosen to be 0.2). From our experience,  $\varepsilon_N^\gamma(\beta)$  changes linearly with  $\beta$  for all the molecules we studied. A cartoon for our  $\beta$ -tuning scheme is shown in Fig. 2, where the red line on the right indicates the gas-phase HOMO calculated using the tuned  $\beta$ .

Our tuning procedure, for a given molecule-metal interface system with  $z$  obtained from a prior DFT calculation, can be summarized as follows:

1. Perform a standard gas-phase OT-RSH calculation for the molecule, i.e., use  $\alpha = 0.2$ ,  $\beta_0 = 1 - \alpha = 0.8$ , and determine  $\gamma$  as in Eq. (3);
2. For the metal slab, compute the image-plane position,  $z_0$ , by matching the long-range XC potential from a local or semi-local functional (PBE in this work) to an image potential. To be specific, first compute the  $xy$ -averaged PBE XC potential for a given metal slab,  $V_{XC}^{PBE}(z)$ , where  $z$  is the variable describing the distance away from the metal sur-

face, then tune the parameter  $z_0$  such that the two curves  $-1/[4(z - z_0)]$  and  $V_{XC}^{PBE}(z)$  have a common tangent point (see Refs. 70,101,102 for details);

3. Compute the approximate polarization induced by the surface with a classical image-charge model by evaluating the expression  $P = 1/[4(z - z_0)]$  (in a.u.), where  $z$  is determined from the geometry of the interface and is the average distance between the molecule and the top layer of the metal slab along the surface normal;
4. Tune the optimal  $\beta$  value according to Eq. (4), using a series of OT-RSH calculations of the gas-phase molecule, with varying  $\beta$  and fixed  $\alpha$  and  $\gamma$ ;
5. Compute the electronic structure of the molecule-metal interface in a self-consistent manner using this OT-RSH functional with the above-determined  $\alpha$ ,  $\beta$ , and  $\gamma$  (in general, each molecule-metal system has its own set of optimal parameters).

In this work, we stop at Step 5. However in principle, one could re-optimize the geometry of the molecule-metal interface, obtain a new  $z$ , and iterate the tuning procedure to self-consistency.

### C. Technical details

All OT-RSH calculations of molecule-metal interfaces are performed using a modified version of Quantum ESPRESSO<sup>103</sup> v. 5.2.0. We implemented long-range screened Fock exchange based on the existing subroutines of short-range screened Fock exchange and hybrid functionals, using norm-conserving pseudopotentials. This is realized via the Fourier transform of the first term in Eq. (1), that is

$$\frac{\alpha + \beta \operatorname{erf}(\gamma |\mathbf{r} - \mathbf{r}'|)}{|\mathbf{r} - \mathbf{r}'|} \xrightarrow{\text{F.T.}} \frac{4\pi}{q^2} \left[ \alpha + \beta \exp\left(-\frac{q^2}{4\gamma^2}\right) \right]. \quad (5)$$

The Gygi-Baldereschi approach<sup>104</sup> is used to treat the Coulomb potential divergence at small  $q$  vectors, as already implemented in Quantum ESPRESSO. A 55 Ry energy cutoff is used for every system. Fock exchange is evaluated using a reduced k-mesh in our calculations; for smaller systems, we verified convergence with respect to the k-mesh. The k-mesh used for each system is specified in Sec. III.

In the current implementation of hybrid functionals in Quantum ESPRESSO, there is an inner self-consistency loop which solves the GKS equation with a fixed Fock operator, and an outer self-consistency loop which updates the Fock operator with new GKS orbitals. Unless noted otherwise, all results shown in this work are from ‘‘perturbative hybrid’’ calculations (which are still self-consistent in a certain sense, see below), in which the Fock operator is constructed only once, using pre-converged PBE orbitals, and the resulting GKS equation

is then solved self-consistently to obtain eigenvalues and orbitals without updating the Fock operator again. The resulting eigenvalues, eigenvectors, and charge density are already different from their PBE counterparts and this self-consistent solution of GKS equation corrects the large errors of PBE in PDOS calculations, in terms of both lineshape and peak positions. Our tests show that this “perturbative hybrid” approach yields almost identical PDOS around the Fermi level compared to fully self-consistent hybrid calculations with both inner and outer loops, but is much more efficient computationally because we omit the outer self-consistency loop.

It is well-known that for transition metals, core-valence interactions may have non-negligible numerical effects in  $GW$ <sup>105</sup> and exact exchange-based<sup>106</sup> calculations of semiconductor band structures. In our tests, the semicore  $sp$ -states of transition metal atoms are found to affect the level alignment by about 0.3 eV. However, explicit inclusion of the semicore  $sp$ -states significantly increases the total number of electrons as well as the required energy cutoff. In order to reduce computational costs, we use a pseudopotential (see Ref. 107 for details) with semicore  $sp$ -states (e.g.,  $4s^2 4p^6 4d^{10} 5s^1$  for Ag) in the valence for the top layer of the transition metal substrate that is closest to the adsorbed molecule, and a pseudopotential without semicore  $sp$ -states (e.g.,  $4d^{10} 5s^1$  for Ag) for the remainder of the metal slab (see Ref. 108 for a note regarding the accuracy of mixing pseudopotentials). In addition, we find that although total energy convergence requires a cutoff of about 200 Ry with explicit semicore  $sp$ -states, the eigenvalues and energy level alignments typically converge at a much lower energy cutoff. The 55 Ry cutoff we use is sufficient for the level alignment of all the systems studied in this work.

The geometries of the molecule-metal interfaces are either adapted from the literature or relaxed using dispersion-corrected XC functionals (see the results section for details), as implemented in VASP<sup>109</sup> with the Projector Augmented Wave (PAW) method<sup>110,111</sup>. We then use the relaxed molecular adsorbate geometry in our gas-phase tuning procedures. Note that this can result in slightly different ( $< 0.1$  eV) HOMO values compared with those obtained from using the molecular geometry optimized in the gas phase. Gas-phase tuning based on Eq. (3) is performed using QChem<sup>112</sup> with a cc-pVTZ basis set, and gas-phase tuning based on Eq. (4) is performed using NWChem<sup>113</sup> with the same basis set.

### III. RESULTS

To demonstrate the success of our approach, we report OT-RSH calculations of six molecule-metal interfaces. We divide them into two categories: systems without significant charge transfer (i.e., physisorbed); and systems with non-negligible charge transfer (i.e., partially chemisorbed). The latter systems feature Fermi level pinning in the PDOS and a significant overlap between the

LUMO resonance peak and  $E_F$ . As discussed in the introduction, the OT-RSH method has repeatedly been found to be highly accurate for gas-phase molecules. Therefore, here we do not dwell on gas-phase results but instead focus on the molecule-surface interaction.

As discussed above, correction schemes that assume weak coupling and do not update the charge density, such as the DFT+ $\Sigma$  approach, are known to perform very well for interfaces in the first category<sup>70</sup>. But a self-consistent method, such as the one presented in this paper, is needed for accurate calculations of the second category. We note that there are specific cases of chemisorption for which charge transfer involves not the frontier, but energetically deeper lying molecular resonances. In such cases, our non-self-consistent scheme may work equally well<sup>64</sup>. For each system, we compare PBE and OT-RSH results with literature results from ultraviolet photoemission spectroscopy (UPS) measurements for both energy level alignment (taken as position of the peak maximum) and work function changes. For the calculated PDOS, a 0.01 Ry broadening is applied to every system, except for the one in Sec. III A 4, where a 0.02 Ry broadening is applied in order to match the experimental PDOS width.

#### A. Systems without significant charge transfer

In this section, we present results for four systems. To begin, we consider benzene adsorbed on Al(111) and 3,4,9,10-perylene-tetracarboxylic-dianhydride (PTCDA) adsorbed on Au(111), two weakly coupled, physisorbed interfaces for which we expect the standard, perturbative DFT+ $\Sigma$  approach to perform well.<sup>70</sup> These systems serve as a proof of concept for the approach proposed in this paper. We then consider 1,4-benzenediamine (BDA) adsorbed on Au(111), where charge transfer is negligible but hybridization between molecular orbitals and Au  $d$ -states is stronger than for the first two systems. In this case, a self-consistent approach such as the one presented here may change the GGA PDOS lineshape, while a post-processing approach, such as the standard DFT+ $\Sigma$ , does not. Finally, we consider Anthracene-2-selenolate (AntSe) adsorbed on Au(111), an even more complicated case as the Se-H bond is replaced by a Se-Au bond upon adsorption, i.e., a new covalent bond is formed.

##### 1. Benzene on Al(111)

Experimental evidence for a rather weak interaction between benzene and Al(111) was given in Ref. 114, where UPS in ultrahigh vacuum was used to determine the energy level alignment. In our calculations of this system, we use a  $4 \times 4$  surface unit cell with 4 layers of Al atoms to represent the slab, and employ a  $4 \times 4 \times 1$  k-mesh ( $2 \times 2 \times 1$  for the Fock exchange contribution). To determine the geometry of this interface, we perform dispersion-corrected DFT calculations using the PBE-

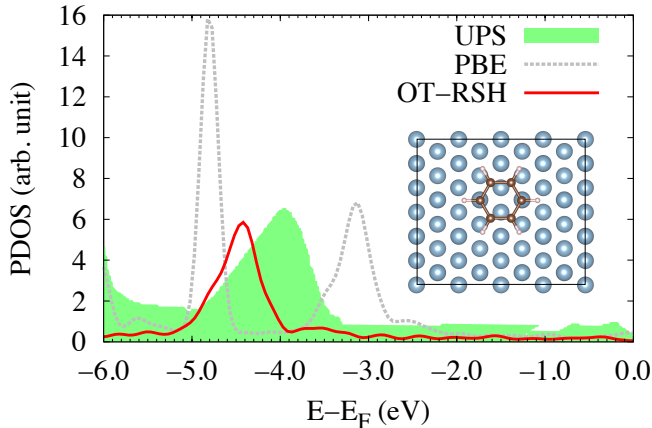


FIG. 3. PDOS of benzene adsorbed on Al(111), whose structure is shown in the inset, as obtained using PBE (grey dashed line) and OT-RSH (red line), compared with results from UPS measurements (green) adapted from Ref. 114.

TS approach (i.e., PBE augmented by the Tkatchenko-Scheffler scheme<sup>115</sup>) including self-consistent screening<sup>116</sup> to capture the impact of the metallic screening on dispersive interactions for a set of fixed molecular geometries at various distances. The lowest total energy is achieved for the molecule lying flat at 3.24 Å above the Al(111) surface on a bridge site.

Following the tuning protocol for interfaces described in Sec. II, Eq. (3) yields  $\gamma = 0.24 \text{ bohr}^{-1}$  and a tuned HOMO energy of -9.4 eV for benzene. For Al(111), the image plane is determined to be 1.1 Å above the surface and, using the optimized distance of our benzene adsorbate, the image-charge energy is then 1.7 eV. In order to incorporate the polarization energy due to the metal surface, we tune  $\beta$  such that the gas-phase HOMO increases by 1.7 eV, based on Eq. (4). This results in an optimal  $\beta$  value of 0.20.

Fig. 3 shows the experimental data for level alignment (as adapted from Ref. 114) and our theoretical results for the PDOS. OT-RSH yields a HOMO resonance at 4.4 eV below  $E_F$ , in much better agreement with experiment (4.0 eV) than PBE (see Fig. 3), which predicts the resonance at 3.1 eV below  $E_F$ . However, PBE and OT-RSH yield essentially the same work function change of -0.3 eV and the same work function of 3.8 eV, suggesting our new OT-RSH scheme leads to results on par with LDA/GGA for predicting accurate work functions and interface dipoles.<sup>53–59</sup> We note that the standard, non-self-consistent DFT+ $\Sigma$  yields a HOMO resonance within 0.1 eV difference from OT-RSH result, as expected for such a weakly coupled interface. We also note that when the vdW-DF2 functional<sup>117</sup> is used to relax the coordinates of the molecule and the top layer of Al(111), the benzene molecule is found at about 3.5 Å above the Al(111) surface, which results in a level alignment of 4.2 eV based on the OT-RSH scheme.

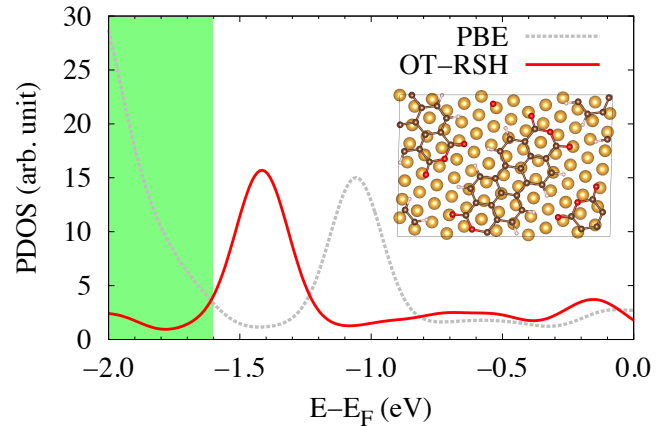


FIG. 4. PDOS of PTCDA adsorbed on Au(111), whose structure is shown in the inset, as obtained using PBE (grey dashed line) and OT-RSH (red line), compared with results from UPS measurements (shown as green shaded area) from Ref. 121.

## 2. PTCDA on Au(111)

PTCDA molecules adsorbed on noble metals have been very well-studied (see Ref. 118 for a detailed review). It is known that the interaction between PTCDA and Au(111) is rather weak<sup>55,118–122</sup>. For consistency with previous work<sup>70</sup>, our calculations use the same geometry as in Ref. 122, where dispersion-corrected functionals yields excellent agreement with experiment for the structure, and 3 layers of Au(111) are used to represent the slab; a  $2 \times 2 \times 1$  k-mesh ( $1 \times 1 \times 1$  for the Fock exchange contribution) is employed.

Following our OT-RSH tuning procedure, in the gas-phase, the optimal  $\gamma$  is 0.16 bohr<sup>-1</sup> and the OT-RSH HOMO is -8.2 eV. For Au(111), the image plane is 0.9 Å above the top surface, as determined in Ref. 70. The average distance between the molecule and the top layer of the surface is 3.18 Å, which yields an image-charge renormalization energy of 1.6 eV. We find that  $\beta = -0.10$  is required to modify the long-range Fock exchange and adjust the gas-phase HOMO energy by 1.6 eV, according to Eq. (4).

Fig. 4 shows our results: OT-RSH yields 1.4 eV for the energy level alignment of the HOMO resonance relative to  $E_F$ , which is reasonably close to the experimental result that is a shoulder in the UPS spectrum centered at 1.8 eV<sup>121</sup>. This is a distinct improvement over the PBE result (ca. 1.1 eV), and matches well with previous DFT+ $\Sigma$  calculations<sup>70</sup>, as expected for weakly coupled interfaces. OT-RSH yields a work function change of -0.7 eV, similar to that of PBE (-0.5 eV) and experiment (-0.5 eV, Ref. 121). For the value of the work function, OT-RSH yields 4.9 eV, in good agreement with PBE and experiment (4.8 eV).

### 3. BDA on Au(111)

BDA adsorbed on Au(111) has attracted considerable attention in both experimental<sup>19,123</sup> and theoretical<sup>36,79,124,125</sup> studies. However, the adsorption geometry has only been revealed recently with scanning tunneling microscopy measurements<sup>123</sup>, which suggest that BDA molecules form self-assembled linear chains on Au(111). Ref. 125 showed that the linear-chain phase of BDA is energetically favored over isolated monomer phases used in previous calculations<sup>36</sup>. In Ref. 125, standard DFT+ $\Sigma$  calculations were performed to correct the PBE PDOS, without altering the PDOS lineshape. Here, we use the same geometry as in Ref. 125, but calculate the PDOS of the interface self-consistently with our new OT-RSH approach. We use 3 layers of Au(111) as the substrate, and a  $4 \times 6 \times 1$  k-mesh ( $2 \times 3 \times 1$  for the Fock exchange contribution).

The tuning approach for the gas-phase molecule, using Eq. (3), yields  $\gamma = 0.23$  bohr<sup>-1</sup> and HOMO at -7.0 eV. As specified above, the image plane of Au(111) is at 0.9 Å above the surface. The average distance between the molecule and the surface is determined to be 3.66 Å. Therefore the polarization due to the substrate is 1.3 eV, based on the image-charge model. Ref. 125 showed that for the linear-chain structure, intermolecular polarization is non-negligible, an effect for the HOMO resonance that amounts to 0.3 eV. Therefore, when choosing  $\beta$  using Eq. (4), we use  $P = 1.6$  eV as the target value, which requires  $\beta = 0.19$ . We note in passing that for the purpose of tuning  $\beta$ , we directly take the intermolecular polarization of 0.3 eV from Ref. 125, without attempting to determine this value from DFT or from classical electrostatic calculations (see Refs. 90,126–129 for such examples).

Fig. 5 shows a comparison of our results to experiment<sup>19</sup>. As can be seen, the OT-RSH HOMO resonance is at about 1.9 eV below  $E_F$ , in much better agreement with experimental results than PBE, which underestimates the level alignment by about 1 eV. We note that in Ref. 125, DFT+ $\Sigma$  was found to place the HOMO at 1.3 eV below  $E_F$ , different from the OT-RSH result in this paper. This is because, firstly, Ref. 125 used an image plane position of 1.47 Å for Au(111), as determined classically from linear response<sup>36,130</sup>, which increases the polarization by 0.3 eV compared to the one determined here. In addition, hybridization of molecular orbitals with metallic states can shift the eigenvalues when taken into account self-consistently, as compared to when using a post-processing approach. Importantly, the DFT+ $\Sigma$  calculations in Ref. 125 only rigidly shifts the PBE PDOS, leaving the lineshape unchanged, in contrast to our OT-RSH approach with its inherent self-consistency when solving the GKS equation. Accordingly, in Fig. 5 one can see that OT-RSH yields a slightly more asymmetric PDOS lineshape, compared to PBE, indicating enhanced hybridization with Au  $d$ -states at lower energy. Lastly, OT-RSH and PBE again yield about the same work function change (-1.5 eV) and the

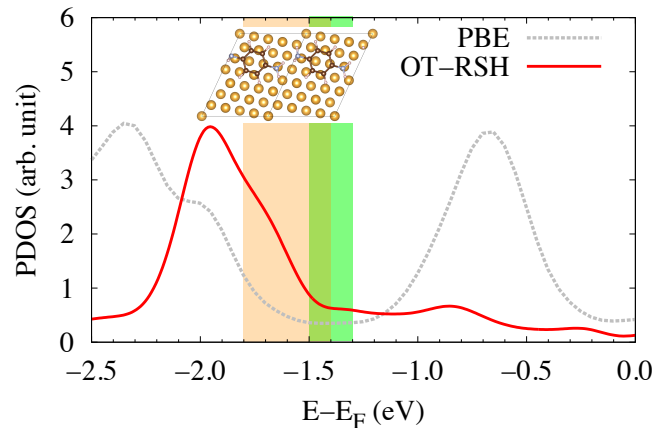


FIG. 5. PDOS of linear-chain phase of BDA on Au(111), whose structure is shown in the inset, as obtained using PBE (grey dashed line) and OT-RSH (red line), compared with results from UPS and x-ray photoemission spectroscopy measurements (green and orange shaded areas, respectively, the width of which represent the experimental uncertainty) from Ref. 19.

same absolute value for the work function (3.8 eV).

### 4. AntSe on Au(111)

AntSe is known to form an upright-standing self-assembled monolayer (SAM) on Au(111)<sup>131</sup>, and is thus different from the other systems studied here. Adsorption of AntSe on Au(111) can be assumed to proceed through cleavage of hydrogen atoms and formation of a covalent Au-Se bond, i.e., it is a chemisorbed system. AntSe on Au(111) has been studied in detail, both experimentally and theoretically, in Ref. 56; the structure we use here was identified as the most likely one in that study, which compared theory results to experimental data from scanning tunneling microscopy. In our calculations, 4 layers of Au(111) serve as the slab, and a  $8 \times 4 \times 1$  k-mesh ( $4 \times 2 \times 1$  for the Fock exchange contribution) is used.

The OT-RSH procedure for this case starts with identifying a suitable gas-phase reference system to determine the optimal RSH parameters. As mentioned above, we assume cleavage of hydrogen atoms upon adsorption, and thus use a H-terminated AntSe molecule (hydrogen optimized using PBE in the gas phase with other atoms fixed) as the reference. The tuning approach for this gas-phase molecule yields an optimal  $\gamma = 0.17$  bohr<sup>-1</sup> and HOMO energy of -7.1 eV. As mentioned before, the location of the Au(111) image plane is 0.9 Å above the surface, and the average distance between the molecule and surface is 7.06 Å. This gives an image-charge energy of 0.6 eV. Similar to the BDA/Au(111) discussed above, due to the small intermolecular distances within the SAM, we expect a non-negligible polarization due



to other molecules, in addition to the polarization due to the metal surface.<sup>50,90,132</sup> As mentioned above, we do not attempt to calculate this contribution from DFT alone. To nevertheless determine this additional intermolecular polarization energy that is responsible for gap difference between an isolated molecule and a SAM, we carry out *GW* calculations (see Ref. 133 for technical details) using the BerkeleyGW<sup>134</sup> package for both the H-terminated gas-phase molecule and the SAM without the metal substrate. We find that the gap is reduced by 1.2 eV in the SAM compared to the gas-phase molecule. However, the convergence of the absolute value of *GW* quasiparticle energies with respect to the vacuum level is very slow and computationally demanding. Furthermore, the dipole moment of AntSe complicates defining a unique vacuum level for the SAM. We therefore make the assumption that this gap change equals  $2P$ , which is reasonable because the shapes of the HOMO and LUMO are similar. It then follows that the HOMO renormalizes in the SAM by 0.6 eV, with respect to the gas-phase molecule. The total renormalization of the HOMO, summing contributions from the substrate and from other molecules, is therefore 1.2 eV, which gives rise to  $\beta = 0.21$  for the interface, according to Eq. (4).

Fig. 6 shows our results compared to experimental data<sup>56</sup> for this system. OT-RSH predicts a HOMO resonance at 1.5 eV below  $E_F$ , in much better agreement with the experimental result (1.9 eV) than PBE, which places the HOMO resonance at 0.8 eV below  $E_F$ . Furthermore, in the OT-RSH PDOS the consecutive features at higher binding energies (lower in energy in Fig. 6) also match the UPS data very well, in sharp contrast to PBE. The good agreement of OT-RSH shows that the gas-phase reference is physically reasonable, meaning that the HOMO orbital is nearly unaffected by the chemisorption, which makes sense given that it is delocalized over the backbone and not localized on the Se linker. Lastly, both OT-RSH and PBE yield excellent agreement with experiment for both the work function change (about 1.3 eV) and its absolute value (3.9 eV in PBE and experiment and 4.0 eV in OT-RSH).

## B. Systems with non-negligible charge transfer

In this section we present two systems involving the Ag(111) substrate with the adsorbates PTCDA and 1,4,5,8-naphthalene-tetracarboxylic dianhydride (NTCDA). Because Ag(111) has a lower work function than Au(111), the coupling between the molecule and substrate is stronger and signatures in UPS that energetically close to the Fermi level are ascribed to the (formerly unoccupied) LUMO of the molecule. This signals non-negligible charge transfer between the metal and the molecule, for which standard DFT+ $\Sigma$  and other non-self-consistent approaches run into difficulties because the weak-coupling assumption of DFT+ $\Sigma$  is violated. In fact, a naive application of DFT+ $\Sigma$  is

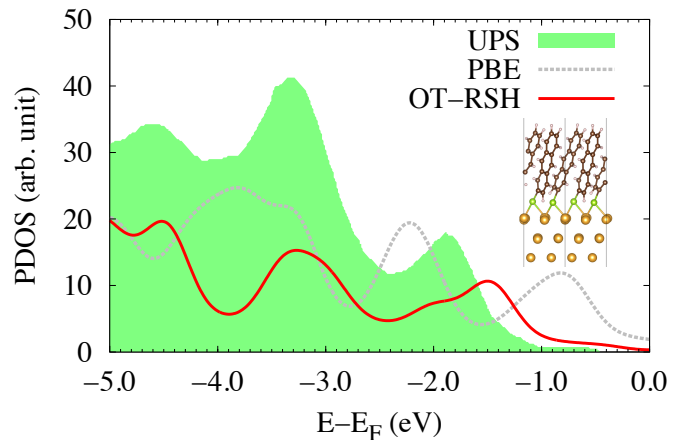


FIG. 6. PDOS of AntSe adsorbed on Au(111), whose structure is shown in the inset, as obtained using PBE (grey dashed line) and OT-RSH (red line), compared with results from UPS measurements (green) taken from Ref. 56.

challenging for the pinned LUMO, which is of course unoccupied in the gas phase, but at least partially occupied when the molecule adsorbs on the metal surface. We will show in the following that our proposed OT-RSH approach also performs well for such cases.

### 1. PTCDA on Ag(111)

PTCDA interacts more strongly with the Ag(111) than with the Au(111) surface and, as observed in UPS and transport experiments, features a LUMO peak pinned a  $E_F$ , see, e.g., Refs. 55,57,118,120,121,135–139 for detailed experimental and theoretical discussions. This charge transfer is already captured by LDA/GGA functionals<sup>55,137</sup>. However, we would expect the LDA/GGA HOMO resonance position (i.e., the second highest peak in energy in UPS) to be higher in energy than the physical one, just as for the cases discussed above. The OT-RSH method proposed in this work, as we will show below, corrects this quantitative error for the HOMO energy alignment, and at the same time maintains a correct description of the LUMO pinning effect. The geometry we use is taken from Ref. 122 and has 3 layers of Ag(111) as the substrate, and we employ a  $2 \times 2 \times 1$  ( $1 \times 1 \times 1$  for the Fock exchange contribution) k-mesh.

For this system, the OT-RSH procedure is the same as discussed above: tuning of gas-phase PTCDA yields an optimal  $\gamma = 0.15$  bohr<sup>-1</sup> and a HOMO energy of -8.1 eV. Note that the gas-phase HOMO energy and optimal  $\gamma$  of PTCDA is slightly different from the one reported above for the PTCDA/Au(111) case, as we use the molecular coordinates optimized for the interface system, which change due to the different interactions with the

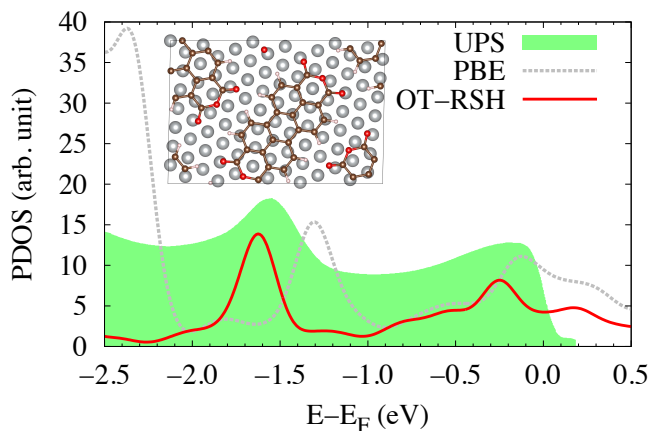


FIG. 7. PDOS of PTCDA adsorbed on Ag(111), whose structure is shown in the inset, as obtained using PBE (grey dashed line) and OT-RSH (red line), compared with results from UPS measurements (green) taken from Ref. 139.

Au or Ag substrate<sup>137</sup>. For Ag(111), the image plane position is determined to be 1.0 Å above the surface. The average distance between PTCDA and the Ag surface is 2.87 Å, giving rise to an image-charge energy of 1.9 eV. When we tune  $\beta$  using Eq. (4) for this adsorbate, a complication arises: with the physically lowest possible  $\beta$ , as specified above ( $\beta = -\alpha = -0.2$ ), the HOMO only increases by 1.7 eV. This is not enough to accommodate the image-charge energy, with the remaining difference being 0.2 eV. This large nonlocal surface polarization is again a sign of strong coupling. In such cases, we simply use  $\beta = -0.2$  to perform the OT-RSH calculation of the interface.

Fig. 7 shows our calculated results for PTCDA adsorbed on Ag(111) compared to data from UPS measurements<sup>139</sup>. The OT-RSH PDOS shows the important feature of LUMO pinning at  $E_F$ , and on top of that corrects the PBE HOMO resonance energy, placing it at 1.6 eV below  $E_F$  and achieving better agreement with experiment. OT-RSH and PBE results for the work function change are both very small and close to zero, comparable to experimental results. Both OT-RSH and PBE yield a work function of 4.6 eV, in good agreement with experiment. These findings are highly encouraging and show that our OT-RSH method captures all the relevant and highly non-trivial effects at this interface.

## 2. NTCDA on Ag(111)

Another interesting system that shows strong interaction is NTCDA adsorbed on Ag(111). Similar to PTCDA on Ag(111), it also features a LUMO peak at  $E_F$ , as evidenced in UPS measurements<sup>140–142</sup>. We relax the NTCDA-Ag(111) geometry with the PBE+vdW<sup>surf</sup> method<sup>122</sup> as implemented in VASP, using 3 layers of

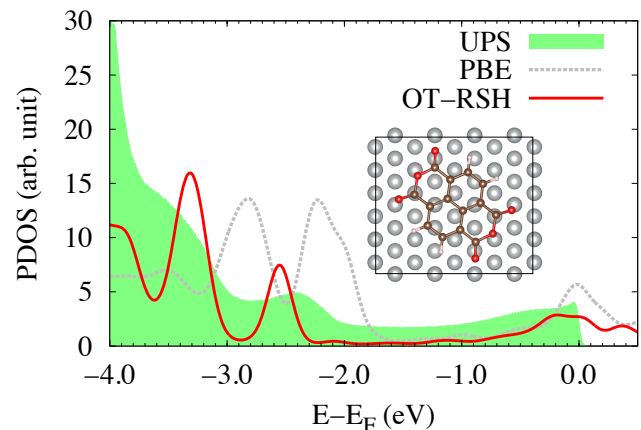


FIG. 8. PDOS of NTCDA adsorbed on Ag(111), whose structure is shown in the inset, as obtained using PBE (grey dashed line) and OT-RSH (red line), compared with results from UPS measurements (green) taken from Ref. 141.

Ag(111) and a  $4 \times 4$  surface unit cell as the substrate. The level alignment calculations are carried out using a  $4 \times 4 \times 1$  k-mesh ( $2 \times 2 \times 1$  for the Fock exchange contribution). From our tuning, the optimal  $\gamma$  for the gas-phase molecule is 0.19 bohr<sup>-1</sup>, according to Eq. (3), and its HOMO energy is -9.7 eV. For Ag(111), the image-plane position is at 1.0 Å above the surface, as determined above. The average distance between the optimized molecule and the surface is 2.88 Å, yielding an image-charge energy of 1.9 eV. This requires  $\beta = -0.082$  for the interface, according to Eq. (4).

Fig. 8 shows our results and UPS data of Ref. 141. Compared to the experimental results, OT-RSH correctly depicts the pinned LUMO, the HOMO resonance, and places the HOMO-1 where UPS shows a shoulder, already around 3.5 eV below  $E_F$ . PBE correctly shows a LUMO pinned at  $E_F$ , describes the HOMO reasonably well, but misplaces the HOMO-1 resonance (by 0.7 eV) with respect to results from OT-RSH and experiment. This strongly suggests that OT-RSH is not only accurate for the frontier resonances, but actually maintains predictive power within several eVs from  $E_F$ ,<sup>84,85</sup> owing to the nonlocal exchange operator<sup>143</sup>. OT-RSH and PBE yield similar work function values (4.7 eV and 4.8 eV, respectively). Regarding the work function change, OT-RSH and PBE differ slightly more (by 0.4 eV and have different signs) in this case. However, we are not aware of experimental data for the work function change in this case, and our results suggest this would be a measurement of interest.

## IV. DISCUSSION

In this paper, we have proposed an approach for accurate calculation of level alignments at molecule-metal

TABLE I. Summary of the OT-RSH and PBE results and experimental literature data for the interface systems studied in this work.  $E_F - E_{\text{HOMO}}$  is the level alignment for the HOMO resonance, and  $\Delta\Phi$  is the work function change compared to the clean metal surface.  $\Phi$  is the resulting work function of the interface. Where we are not aware of an experimental  $\Delta\Phi$  or  $\Phi$  value, an “x” sign is used.  $\gamma$  denotes the optimally-tuned range-separation parameter based on Eq. (3) and is in bohr<sup>-1</sup>.  $\epsilon_{\text{HOMO}}^{\text{OT-RSH}}$  is the gas-phase OT-RSH HOMO energy.  $z_0$  is the DFT-determined image-plane position for the metal surface.  $P$  is the surface polarization calculated using an image-charge model. For systems with small surface unit cells, such as BDA/Au(111) and AntSe/Au(111),  $P$  also includes polarization contribution due to other molecules in the molecular layer.  $\beta$  is tuned according to Eq. (4) and is used for the calculation of the interface. The first four systems show negligible charge transfer and are discussed in Sec. III A. The last two systems show significant charge transfer and are discussed in Sec. III B.

	$E_F - E_{\text{HOMO}}$ (eV)			$\Delta\Phi$ [ $\Phi$ ] (eV)			$\gamma(a_0^{-1})$	$\epsilon_{\text{HOMO}}^{\text{OT-RSH}}$ (eV)	$z_0$ (Å)	$P$ (eV)	$\beta$	comment
	PBE	OT-RSH	Expt.	PBE	OT-RSH	Expt.						
Benzene/Al(111)	3.1	4.4	4.0 <sup>114</sup>	-0.3 [3.8]	-0.3 [3.8]	-0.2 [x] <sup>114</sup>	0.24	-9.4	1.1	1.7	0.20	weak physisorption
PTCDA/Au(111)	1.1	1.4	1.6-2.0 <sup>121</sup>	-0.5 [4.8]	-0.7 [4.9]	-0.5 [4.8] <sup>121</sup>	0.16	-8.2	0.9	1.6	-0.10	weak physisorption
BDA/Au(111)	0.7	1.9	1.3-1.8 <sup>19</sup>	-1.5 [3.8]	-1.6 [3.8]	x [x]	0.23	-7.0	0.9	1.6	0.19	stronger hybridization
AntSe/Au(111)	0.8	1.5	1.9 <sup>56</sup>	-1.4 [3.9]	-1.5 [4.0]	-1.3 [3.9] <sup>56</sup>	0.17	-7.1	0.9	1.2	0.21	with covalent bond
PTCDA/Ag(111)	1.3	1.6	1.5 <sup>139</sup>	+0.1 [4.6]	0.0 [4.6]	-0.1 [4.8] <sup>121</sup> , 0.1 [4.9] <sup>135</sup>	0.15	-8.1	1.0	1.9	-0.20	Fermi level pinning
NTCDA/Ag(111)	2.2	2.5	2.4 <sup>141</sup>	+0.2 [4.8]	-0.2 [4.7]	x [x]	0.19	-9.7	1.0	1.9	-0.082	Fermi level pinning

interfaces based on the OT-RSH functional, and tested it for a set of well-studied and complex systems. Our results, summarized in Table I, show that this method is successful in quantitative predictions of energy level alignment. To understand its success, we refer again to Fig. 2 and compare it to Fig. 1: The essential idea of our OT-RSH approach is to tune the parameter  $\beta$  and adapt the long-range Fock exchange to capture the screening due to the metal surface. The amount of screening and the choice of  $\beta$  are determined by  $P$ , given in Eq. (4). In Fig. 2, the red lines on the right demonstrate the attempted gas-phase HOMO/LUMO energy with the tuned  $\beta$  value, and the red curve on the left shows the resulting PDOS of the molecule in the interface. In Eq. (4), for the systems studied here the left hand side is almost linear in  $\beta$ , which means that the tuned  $\beta$  value, as well as the resulting level alignment at the interface, are not sensitive to small variations of  $P$ .

With our method we set out to capture physics inherent to *GW* calculations but absent from currently available DFT approaches for interfaces, namely a sensitivity of XC effects to the dielectric environment specific to molecule-metal interfaces. The uneven performance of standard DFT approaches for interfaces, i.e., the success in describing work functions and interface dipoles but the failures in predicting level alignments, can be understood from the “nearsightedness principle” of many-electron systems<sup>144</sup>. It states that many important static physical quantities, including the density, only depend on changes in the potential at nearby points. This explains the success of local and semi-local XC functionals in predicting the density of molecule-metal systems and highly relevant quantities that are directly determined from it, notably total energies, work functions, and interface dipoles. However, long-range Coulomb interactions are an exception to this principle. They are important for molecule-metal interfaces, especially considering the renormalization of molecular resonances due to the metal surface. Because of the long-range nature of the phenomenon, a standard hybrid functional without

range separation, or a range-separated hybrid functional without long-range Fock exchange, cannot in general capture the image-charge effect accurately. Therefore, we choose to adapt the long-range part of the XC potential by tuning  $\beta$  to capture  $P$ , thereby implicitly including the otherwise missing distance-dependent screening in our approach, which is crucial for its success. At the same time, we deliberately do not modify the short-range part of the XC potential (controlled by  $\alpha$  and  $\gamma$ ) when going from the gas phase to the surface. Importantly, orbital energies and resonances are expected to respond to  $\beta$  tuning, but the density and quantities that are directly determined from it are expected to be mostly unchanged. This reasoning is strongly supported by our results of level alignments and work function changes. Our scheme therefore provides a superior GKS approach that can predict both energy level alignments and work function changes with high accuracy.

As we have stressed throughout this paper, one advantage of our fully self-consistent approach, as compared to DFT+ $\Sigma$  and other non-self-consistent schemes, is that it calculates and fully captures the hybridization between the molecule and the metal. Therefore, it can alter the PBE PDOS lineshape and is also applicable to systems with stronger charge transfer and Fermi level pinning. In addition, since it is based on GKS and includes a fraction of short-range Fock exchange, it can also yield improved relative orbital spacing, as shown in the examples of AntSe/Au(111) and NTCDA/Ag(111), as well as improved orbital ordering, as was demonstrated previously for other systems<sup>58,85,92,145–147</sup>.

In spite of its success, we also would like to point out that the method proposed here is not a panacea. In particular, we focused here on the level alignment and PDOS of the molecule, and did not discuss how the specific choice of  $\alpha$ ,  $\beta$ , and  $\gamma$  may affect specifics in the electronic structure of the metal substrate. In this context, we would like to mention that full Fock exchange often artificially opens a gap for metals<sup>148</sup>, and that many hybrid functionals perform worse than local and semi-local func-

tionals for metals<sup>149</sup>. We expect that similar situations may occur when one has to choose a large  $\beta$  value following the tuning procedure. Coincidentally, this is not the case for the systems studied in this work. The largest  $\beta$  used in this work is about 0.2, and with this amount of long-range Fock exchange the PDOS of the metal substrate stays qualitatively correct. Quantitatively, even for a rather small amount of Fock exchange, the theoretical description of certain properties of real metals may suffer<sup>79</sup>.

Another limitation is that for PTCDA/Ag(111), and perhaps also other systems, with the physically lowest possible value for  $\beta$ , i.e.,  $\beta = -\alpha = -0.2$  the left hand side is smaller than the right hand side of Eq. (4). In other words, we cannot accommodate the full magnitude of  $P$  by tuning  $\beta$ . For PTCDA/Ag(111), the remaining difference was small. However, one may imagine molecule-metal systems where the deficit is somewhat larger, and using  $\beta = -0.2$  would not be enough. These scenarios are more likely to occur for more strongly coupled interfaces, such as pentacene adsorbed on Ag or Cu<sup>150</sup>. In those cases, the currently proposed OT-RSH approach may not work as well as for the systems shown in this paper.

Lastly, we have used a DFT-based image-charge model to approximate the otherwise rather complicated change in the Coulomb screening induced by the metal surface. As far as this particular approximation is concerned, the approach proposed in this work shares the same advantages and disadvantages as the “standard” DFT+ $\Sigma$  method: The image-charge interaction mimics static (frequency-independent) polarization, and misses dynamical (frequency-dependent) surface polarization effects and the polarization of the molecule due to the metal, which is a higher order effect. Moreover, for cases of non-negligible intermolecular polarization such as polarizable SAMs, so far we did not attempt to compute this solely from DFT, but for this proof-of-principle study relied on *GW* results.

One way of understanding the above limitations is to realize that molecule-metal interfaces are indeed strongly heterogeneous systems in the sense that the screening perpendicular to the surface is strongly distance-dependent and very different from the screening parallel to it. In the OT-RSH approach proposed here, we use *scalar* parameters,  $\alpha$ ,  $\beta$ , and  $\gamma$ , which may not be enough for complicated cases. Work along the lines of “local hybrids”<sup>151</sup>, i.e., spatially dependent parameters  $\alpha(\mathbf{r})$ ,  $\beta(\mathbf{r})$ , or even  $\gamma(\mathbf{r})$ , as well as density-based mixing parameters<sup>152</sup>, may describe the heterogeneous environment more accurately. But the construction of such functionals and their implementations may prove to be much more difficult.

## V. CONCLUSION

In this work, we developed an approach to calculate the energy level alignment at molecule-metal interfaces with good accuracy, based on an OT-RSH functional. The essential idea is to start with an accurate electronic structure description in the gas phase and capture the nonlocal surface polarization due to the metal by screening the long-range Fock exchange. We proposed a non-empirical way to tune the long-range Fock exchange per molecule-metal pair based on an image-charge model, and implemented this approach in a plane-wave code. Results from our fully self-consistent approach for several prototypical, challenging molecule-metal interfaces are in quantitative agreement with experiments, for both the level alignments and work function changes. Keeping its remaining limitations as discussed in this paper in mind, we believe that our OT-RSH approach paves the way for accurate and reliable predictions of energetics and level alignments at heterogeneous interfaces, especially those related to energy conversion and molecular electronics. Finally, we note that the efficiency of these calculations strongly depends on new algorithm developments for computing nonlocal Fock exchange, such as the recently proposed adaptively compressed exchange operator method<sup>153</sup>.

## VI. ACKNOWLEDGEMENT

We thank Achim Schöll for providing us the experimental data for NTCDA adsorbed on Ag(111) that is published in Ref. 141. Work in Berkeley was supported by the U.S. Department of Energy, Office of Basic Energy Sciences, Division of Materials Sciences and Engineering under Contract No. DE-AC02-05CH11231. Work performed at the Molecular Foundry was also supported by the Office of Science, Office of Basic Energy Sciences, of the U.S. Department of Energy under the same contract number. Work in Rehovoth was supported by the European Research Council, the Israel Science Foundation, the United States-Israel Binational Science Foundation, the Wolfson Foundation, the Austrian Science Fund (FWF):J3608-N20, and the Molecular Foundry. We thank the National Energy Research Scientific Computing center for computational resources.

- <sup>1</sup>H. Ishii, K. Sugiyama, E. Ito, and K. Seki, *Adv. Mater.* **11**, 605 (1999).
- <sup>2</sup>A. Kahn, N. Koch, and W. Gao, *J. Polym. Sci., Part B: Polym. Phys.* **41**, 2529 (2003).
- <sup>3</sup>N. Koch, *Chem. Phys. Chem.* **8**, 1438 (2007).
- <sup>4</sup>N. Ueno and S. Kera, *Prog. Surf. Sci.* **83**, 490 (2008).
- <sup>5</sup>J. Hwang, A. Wan, and A. Kahn, *Mater. Sci. Eng., R* **64**, 1 (2009).
- <sup>6</sup>S. Braun, W. R. Salaneck, and M. Fahlman, *Adv. Mater.* **21**, 1450 (2009).
- <sup>7</sup>N. Koch, N. Ueno, and A. T. S. Wee, eds., *The Molecule-Metal Interface* (Wiley-VCH, 2013).



- <sup>8</sup>W. Liu, A. Tkatchenko, and M. Scheffler, *Acc. Chem. Res.* **47**, 3369 (2014).
- <sup>9</sup>M. Willenbockel, D. Luftner, B. Stadtmüller, G. Koller, C. Kumpf, S. Soubatch, P. Puschnig, M. G. Ramsey, and F. S. Tautz, *Phys. Chem. Chem. Phys.* **17**, 1530 (2015).
- <sup>10</sup>R. J. Maurer, V. G. Ruiz, J. Camarillo-Cisneros, W. Liu, N. Ferri, K. Reuter, and A. Tkatchenko, *Prog. Surf. Sci.* **91**, 72 (2016).
- <sup>11</sup>N. D. Lang, *Phys. Rev. B* **4**, 4234 (1971).
- <sup>12</sup>S. Y. Quek, L. Venkataraman, H. J. Choi, S. G. Louie, M. S. Hybertsen, and J. B. Neaton, *Nano Lett.* **7**, 3477 (2007).
- <sup>13</sup>Y. Xue, S. Datta, and M. A. Ratner, *J. Chem. Phys.* **115**, 4292 (2001).
- <sup>14</sup>M. A. Reed, C. Zhou, C. J. Müller, T. P. Burgin, and J. M. Tour, *Science* **278**, 252 (1997).
- <sup>15</sup>N. J. Tao, *Nature Nanotech.* **1**, 173 (2006).
- <sup>16</sup>L. Venkataraman, J. E. Klare, C. Nuckolls, M. S. Hybertsen, and M. L. Steigerwald, *Nature* **442**, 904 (2006).
- <sup>17</sup>A. C. Dürr, N. Koch, M. Kelsch, A. Rühm, J. Ghijsen, R. L. Johnson, J.-J. Pireaux, J. Schwartz, F. Schreiber, H. Dosch, and A. Kahn, *Phys. Rev. B* **68**, 115428 (2003).
- <sup>18</sup>S. Y. Quek, M. Kamenetska, M. L. Steigerwald, H. J. Choi, S. G. Louie, M. S. Hybertsen, J. B. Neaton, and L. Venkataraman, *Nature Nanotechnology* **4**, 230 (2009).
- <sup>19</sup>M. Dell'Angela, G. Kladnik, A. Cossaro, A. Verdini, M. Kamenetska, I. Tamblin, S. Y. Quek, J. B. Neaton, D. Cvetko, A. Morgante, and L. Venkataraman, *Nano Lett.* **10**, 2470 (2010).
- <sup>20</sup>L. Hedin, *Phys. Rev.* **139**, A796 (1965).
- <sup>21</sup>M. S. Hybertsen and S. G. Louie, *Phys. Rev. B* **34**, 5390 (1986).
- <sup>22</sup>X. Blase, C. Attaccalite, and V. Olevano, *Phys. Rev. B* **83**, 115103 (2011).
- <sup>23</sup>S. Sharifzadeh, I. Tamblin, P. Doak, P. T. Darancet, and J. B. Neaton, *Eur. Phys. J. B* **85**, 323 (2012).
- <sup>24</sup>C. Faber, C. Attaccalite, V. Olevano, E. Runge, and X. Blase, *Phys. Rev. B* **83**, 115123 (2011).
- <sup>25</sup>C. Faber, P. Boulanger, C. Attaccalite, I. Duchemin, and X. Blase, *Philos. Trans. R. Soc. Lond. A-Math. Phys. Eng. Sci.* **372** (2014).
- <sup>26</sup>M. J. van Setten, F. Caruso, S. Sharifzadeh, X. Ren, M. Scheffler, F. Liu, J. Lischner, L. Lin, J. R. Deslippe, S. G. Louie, C. Yang, F. Weigend, J. B. Neaton, F. Evers, and P. Rinke, *J. Chem. Theory Comput.* **11**, 5665 (2015).
- <sup>27</sup>F. Kaplan, M. E. Harding, C. Seiler, F. Weigend, F. Evers, and M. J. van Setten, *J. Chem. Theory Comput.* **12**, 2528 (2016).
- <sup>28</sup>M. S. Hybertsen and S. G. Louie, *Phys. Rev. Lett.* **55**, 1418 (1985).
- <sup>29</sup>W. G. Aulbur, L. Jönsson, and J. W. Wilkins, in *Solid State Physics*, Vol. 54, edited by H. Ehrenreich and S. Spaepen (Academic Press, 2000) pp. 1 – 218.
- <sup>30</sup>P. Rinke, A. Qteish, J. Neugebauer, C. Freysoldt, and M. Scheffler, *New J. Phys.* **7**, 126 (2005).
- <sup>31</sup>Y. Li, D. Lu, S. A. Swanson, J. C. Scott, and G. Galli, *J. Phys. Chem. C* **112**, 6413 (2008).
- <sup>32</sup>N. Kharche, J. T. Muckerman, and M. S. Hybertsen, *Phys. Rev. Lett.* **113**, 176802 (2014).
- <sup>33</sup>C. Draxl, D. Nabok, and K. Hannewald, *Acc. Chem. Res.* **47**, 3225 (2014).
- <sup>34</sup>M. Strange and K. S. Thygesen, *Phys. Rev. B* **86**, 195121 (2012).
- <sup>35</sup>M. van Schilfgaarde, T. Kotani, and S. V. Faleev, *Phys. Rev. B* **74**, 245125 (2006).
- <sup>36</sup>I. Tamblin, P. Darancet, S. Y. Quek, S. Bonev, and J. B. Neaton, *Phys. Rev. B* **84**, 201402 (2011).
- <sup>37</sup>P. Rinke, A. Qteish, J. Neugebauer, and M. Scheffler, *Phys. Status Solidi B* **245**, 929 (2008).
- <sup>38</sup>F. Bruneval and M. A. L. Marques, *J. Chem. Theory Comput.* **9**, 324 (2013).
- <sup>39</sup>P. Hohenberg and W. Kohn, *Phys. Rev.* **136**, B864 (1964).
- <sup>40</sup>W. Kohn and L. J. Sham, *Phys. Rev.* **140**, A1133 (1965).
- <sup>41</sup>D. P. Chong, O. V. Gritsenko, and E. J. Baerends, *J. Chem. Phys.* **116**, 1760 (2002).
- <sup>42</sup>C.-O. Almbladh and U. von Barth, *Phys. Rev. B* **31**, 3231 (1985).
- <sup>43</sup>L. Kronik, T. Stein, S. Refaely-Abramson, and R. Baer, *J. Chem. Theory Comput.* **8**, 1515 (2012).
- <sup>44</sup>L. Kronik and S. Kümmel, *Top. Curr. Chem.* **347**, 137 (2014).
- <sup>45</sup>J. P. Perdew, R. G. Parr, M. Levy, and J. L. Balduz, *Phys. Rev. Lett.* **49**, 1691 (1982).
- <sup>46</sup>J. P. Perdew and M. Levy, *Phys. Rev. Lett.* **51**, 1884 (1983).
- <sup>47</sup>L. J. Sham and M. Schlüter, *Phys. Rev. Lett.* **51**, 1888 (1983).
- <sup>48</sup>S. Kümmel and L. Kronik, *Rev. Mod. Phys.* **80**, 3 (2008).
- <sup>49</sup>J. C. Inkson, *J. Phys. C* **6**, 1350 (1973).
- <sup>50</sup>J. B. Neaton, M. S. Hybertsen, and S. G. Louie, *Phys. Rev. Lett.* **97**, 216405 (2006).
- <sup>51</sup>J. M. Garcia-Lastra, C. Rostgaard, A. Rubio, and K. S. Thygesen, *Phys. Rev. B* **80**, 245427 (2009).
- <sup>52</sup>C. Freysoldt, P. Rinke, and M. Scheffler, *Phys. Rev. Lett.* **103**, 056803 (2009).
- <sup>53</sup>V. De Renzi, R. Rousseau, D. Marchetto, R. Biagi, S. Scandolo, and U. del Pennino, *Phys. Rev. Lett.* **95**, 046804 (2005).
- <sup>54</sup>I. Magid, L. Burstein, O. Seitz, L. Segev, L. Kronik, and Y. Rosenwaks, *J. Phys. Chem. C* **112**, 7145 (2008).
- <sup>55</sup>L. Romaner, D. Nabok, P. Puschnig, E. Zojer, and C. Ambrosch-Draxl, *New J. Phys.* **11**, 053010 (2009).
- <sup>56</sup>A. M. Track, F. Rissner, G. Heimel, L. Romaner, D. Käfer, A. Bashir, G. M. Rangger, O. T. Hofmann, T. Bučko, G. Witte, and E. Zojer, *J. Phys. Chem. C* **114**, 2677 (2010).
- <sup>57</sup>O. T. Hofmann, V. Atalla, N. Moll, P. Rinke, and M. Scheffler, *New J. Phys.* **15**, 123028 (2013).
- <sup>58</sup>Y. Huang, E. Wruss, D. Egger, S. Kera, N. Ueno, W. Saidi, T. Bucko, A. Wee, and E. Zojer, *Molecules* **19** (2014).
- <sup>59</sup>T. Abu-Husein, S. Schuster, D. A. Egger, M. Kind, T. Santowski, A. Wiesner, R. Chiechi, E. Zojer, A. Terfort, and M. Zharnikov, *Adv. Func. Mater.* **25**, 3943 (2015).
- <sup>60</sup>F. Flores, J. Ortega, and H. Vazquez, *Phys. Chem. Chem. Phys.* **11**, 8658 (2009).
- <sup>61</sup>M. Rohlfing, *Phys. Rev. B* **82**, 205127 (2010).
- <sup>62</sup>A. Greuling, M. Rohlfing, R. Temirov, F. S. Tautz, and F. B. Anders, *Phys. Rev. B* **84**, 125413 (2011).
- <sup>63</sup>A. M. Souza, I. Rungger, C. D. Pemmaraju, U. Schwingenschloegl, and S. Sanvito, *Phys. Rev. B* **88**, 165112 (2013).
- <sup>64</sup>M. Yu, P. Doak, I. Tamblin, and J. B. Neaton, *J. Phys. Chem. Lett.* **4**, 1701 (2013).
- <sup>65</sup>A. Migani, D. J. Mowbray, J. Zhao, H. Petek, and A. Rubio, *J. Chem. Theory Comput.* **10**, 2103 (2014).
- <sup>66</sup>T. Esat, T. Deilmann, B. Lechtenberg, C. Wagner, P. Krüger, R. Temirov, F. B. Anders, M. Rohlfing, and F. S. Tautz, *Phys. Rev. B* **91**, 144415 (2015).
- <sup>67</sup>J. E. Moore and L. Jensen, *J. Phys. Chem. C* **120**, 5659 (2016).
- <sup>68</sup>S. Roychoudhury, C. Motta, and S. Sanvito, *Phys. Rev. B* **93**, 045130 (2016).
- <sup>69</sup>J. Ma, Z.-F. Liu, J. B. Neaton, and L.-W. Wang, *Appl. Phys. Lett.* **108**, 262104 (2016).
- <sup>70</sup>D. A. Egger, Z.-F. Liu, J. B. Neaton, and L. Kronik, *Nano Lett.* **15**, 2448 (2015).
- <sup>71</sup>H. Vázquez, R. Oszwaldowski, P. Pou, J. Ortega, R. Pérez, F. Flores, and A. Kahn, *Eur. Phys. Lett.* **65**, 802 (2004).
- <sup>72</sup>G. Heimel, S. Duhm, I. Salzmann, A. Gerlach, A. Strozbecka, J. Niederhausen, C. Bürker, T. Hosokai, I. Fernandez-Torrente, G. Schulze, S. Winkler, A. Wilke, R. Schlesinger, J. Frisch, B. Bröker, A. Vollmer, B. Detlefs, J. Pflaum, S. Kera, K. J. Franke, N. Ueno, J. I. Pascual, F. Schreiber, and N. Koch, *Nat. Chem.* **5**, 187 (2013).
- <sup>73</sup>G. Heimel, L. Romaner, J.-L. Brédas, and E. Zojer, *Phys. Rev. Lett.* **96**, 196806 (2006).
- <sup>74</sup>A. d. M. Souza, I. Rungger, R. B. Pontes, A. R. Rocha, A. J. Roque da Silva, U. Schwingenschloegl, and S. Sanvito, *Nanoscale* **6**, 14495 (2014).

- <sup>75</sup>T. Rangel, G.-M. Rignanese, and V. Olevano, *Beilstein J. Nanotechnol.* **6**, 1247 (2015).
- <sup>76</sup>A. Seidl, A. Görling, P. Vogl, J. A. Majewski, and M. Levy, *Phys. Rev. B* **53**, 3764 (1996).
- <sup>77</sup>A. D. Becke, *J. Chem. Phys.* **98**, 5648 (1993).
- <sup>78</sup>J. Heyd, J. E. Peralta, G. E. Scuseria, and R. L. Martin, *J. Chem. Phys.* **123**, 174101 (2005).
- <sup>79</sup>A. Biller, I. Tamblyn, J. B. Neaton, and L. Kronik, *J. Chem. Phys.* **135**, 164706 (2011).
- <sup>80</sup>R. Baer, E. Livshits, and U. Salzner, *Annu. Rev. Phys. Chem.* **61**, 85 (2010).
- <sup>81</sup>T. Stein, H. Eisenberg, L. Kronik, and R. Baer, *Phys. Rev. Lett.* **105**, 266802 (2010).
- <sup>82</sup>S. Refaely-Abramson, R. Baer, and L. Kronik, *Phys. Rev. B* **84**, 075144 (2011).
- <sup>83</sup>T. Körzdörfer, J. S. Sears, C. Sutton, and J.-L. Brédas, *J. Chem. Phys.* **135**, 204107 (2011).
- <sup>84</sup>S. Refaely-Abramson, S. Sharifzadeh, N. Govind, J. Autschbach, J. B. Neaton, R. Baer, and L. Kronik, *Phys. Rev. Lett.* **109**, 226405 (2012).
- <sup>85</sup>D. A. Egger, S. Weissman, S. Refaely-Abramson, S. Sharifzadeh, M. Dauth, R. Baer, S. Kümmel, J. B. Neaton, E. Zojer, and L. Kronik, *J. Chem. Theory Comp.* **10**, 1934 (2014).
- <sup>86</sup>H. Phillips, Z. Zheng, E. Geva, and B. D. Dunietz, *Org. Electr.* **15**, 1509 (2014).
- <sup>87</sup>I. Tamblyn, S. Refaely-Abramson, J. B. Neaton, and L. Kronik, *J. Phys. Chem. Lett.* **5**, 2734 (2014).
- <sup>88</sup>T. Körzdörfer and J.-L. Brédas, *Acc. Chem. Res.* **47**, 3284 (2014).
- <sup>89</sup>J. Autschbach and M. Srebro, *Acc. Chem. Res.* **47**, 2592 (2014).
- <sup>90</sup>S. Refaely-Abramson, S. Sharifzadeh, M. Jain, R. Baer, J. B. Neaton, and L. Kronik, *Phys. Rev. B* **88**, 081204(R) (2013).
- <sup>91</sup>L. Kronik and J. B. Neaton, *Annu. Rev. Phys. Chem.* **67**, 587 (2016).
- <sup>92</sup>Z.-F. Liu, S. Wei, H. Yoon, O. Adak, I. Ponce, Y. Jiang, W.-D. Jang, L. M. Campos, L. Venkataraman, and J. B. Neaton, *Nano Lett.* **14**, 5365 (2014).
- <sup>93</sup>A. Yamada, Q. Feng, A. Hoskins, K. D. Fenk, and B. D. Dunietz, *Nano Lett.* **16**, 6092 (2016).
- <sup>94</sup>J. Toulouse, F. Colonna, and A. Savin, *Phys. Rev. A* **70**, 062505 (2004).
- <sup>95</sup>T. Yanai, D. P. Tew, and N. C. Handy, *Chem. Phys. Lett.* **393**, 51 (2004).
- <sup>96</sup>J. P. Perdew, K. Burke, and M. Ernzerhof, *Phys. Rev. Lett.* **77**, 3865 (1996); *ibid.*, **78**, 1396(E) (1997).
- <sup>97</sup>T. M. Henderson, B. G. Janesko, and G. E. Scuseria, *J. Chem. Phys.* **128**, 194105 (2008).
- <sup>98</sup>D. Lüftner, S. Refaely-Abramson, M. Pachler, R. Resel, M. G. Ramsey, L. Kronik, and P. Puschnig, *Phys. Rev. B* **90**, 075204 (2014).
- <sup>99</sup>S. Refaely-Abramson, M. Jain, S. Sharifzadeh, J. B. Neaton, and L. Kronik, *Phys. Rev. B* **92**, 081204 (2015).
- <sup>100</sup>J. Heyd, G. E. Scuseria, and M. Ernzerhof, *J. Chem. Phys.* **118**, 8207 (2003); *ibid.*, **124**, 219906(E) (2006).
- <sup>101</sup>A. G. Egiluz and W. Hanke, *Phys. Rev. B* **39**, 10433(R) (1989).
- <sup>102</sup>Y. Li, D. Lu, and G. Galli, *J. Chem. Theory Comput.* **5**, 881 (2009).
- <sup>103</sup>P. Giannozzi *et al.*, *J. Phys.: Condens. Matter* **21**, 395502 (2009).
- <sup>104</sup>F. Gygi and A. Baldereschi, *Phys. Rev. B* **34**, 4405(R) (1986).
- <sup>105</sup>A. Marini, G. Onida, and R. Del Sole, *Phys. Rev. Lett.* **88**, 016403 (2002).
- <sup>106</sup>S. Sharma, J. K. Dewhurst, and C. Ambrosch-Draxl, *Phys. Rev. Lett.* **95**, 136402 (2005).
- <sup>107</sup>We create norm-conserving Ag and Au pseudopotentials using the LD1 utility of Quantum ESPRESSO. For Ag with semicore states, the  $r_c$  values for 4s, 4p, and 4d orbitals are 1.0, 1.8, and 1.2 a.u., respectively. For Ag without semicore states, the  $r_c$  for 4d, 5s, and 5p orbitals are all 2.4 a.u. For Au with semicore states, the  $r_c$  for 5s, 5p, and 5d orbitals are 1.03, 2.3, and 2.3 a.u., respectively. For Au without semicore states, the  $r_c$  for 5d, 6s, and 6p orbitals are all 2.54 a.u. For pseudopotentials of all other elements, we use those that are originally created using FHI98PP and are converted to UPF format, as found on Quantum ESPRESSO website: <http://www.quantum-espresso.org/pseudopotentials/>.
- <sup>108</sup>We have checked the effect of mixing these two types of pseudopotentials on the level alignment, using the system of 2,3,5,6-tetrafluoro-7,7,8,8-tetracyano-quinodimethane (F4TCNQ) adsorbed on Ag(111) surface. The calculation is performed using HSE functional and the resulting level alignment is in quantitative agreement with both PAW calculations in VASP and the published results in Ref. 57 using the same functional.
- <sup>109</sup>G. Kresse and J. Hafner, *Phys. Rev. B* **47**, 558 (1993); *ibid.*, **49**, 14251 (1994); G. Kresse and J. Furthmüller, *Comput. Mat. Sci.* **6**, 15 (1996); *Phys. Rev. B* **54**, 11169 (1996).
- <sup>110</sup>P. E. Blöchl, *Phys. Rev. B* **50**, 17953 (1994).
- <sup>111</sup>G. Kresse and D. Joubert, *Phys. Rev. B* **59**, 1758 (1999).
- <sup>112</sup>Y. Shao *et al.*, *Mol. Phys.* **113**, 184 (2014).
- <sup>113</sup>M. Valiev, E. J. Bylaska, N. Govind, K. Kowalski, T. P. Straatsma, H. J. J. van Dam, D. Wang, J. Nieplocha, E. Apra, T. L. Windus, and W. A. de Jong, *Comput. Phys. Commun.* **181**, 1477 (2010).
- <sup>114</sup>R. Duschek, F. Mittendorfer, R. I. R. Blyth, F. P. Netzer, J. Hafner, and M. G. Ramsey, *Chem. Phys. Lett.* **318**, 43 (2000).
- <sup>115</sup>A. Tkatchenko and M. Scheffler, *Phys. Rev. Lett.* **102**, 073005 (2009).
- <sup>116</sup>A. Tkatchenko, R. A. DiStasio, Jr., R. Car, and M. Scheffler, *Phys. Rev. Lett.* **108**, 236402 (2012).
- <sup>117</sup>K. Lee, É. D. Murray, L. Kong, B. I. Lundqvist, and D. C. Langreth, *Phys. Rev. B* **82**, 081101(R) (2010).
- <sup>118</sup>F. Tautz, *Prog. Surf. Sci.* **82**, 479 (2007).
- <sup>119</sup>H. Vázquez, R. Oszwaldowski, P. Pou, J. Ortega, R. Pérez, F. Flores, and A. Kahn, *Europhys. Lett.* **65**, 802 (2004).
- <sup>120</sup>S. K. M. Henze, O. Bauer, T.-L. Lee, M. Sokolowski, and F. Tautz, *Surf. Sci.* **601**, 1566 (2007).
- <sup>121</sup>S. Duhm, A. Gerlach, I. Salzmann, B. Bröker, R. L. Johnson, F. Schreiber, and N. Koch, *Org. Electron.* **9**, 111 (2008).
- <sup>122</sup>V. G. Ruiz, W. Liu, E. Zojer, M. Scheffler, and A. Tkatchenko, *Phys. Rev. Lett.* **108**, 146103 (2012).
- <sup>123</sup>T. K. Haxton, H. Zhou, I. Tamblyn, D. Eom, Z. Hu, J. B. Neaton, T. F. Heinz, and S. Whitelam, *Phys. Rev. Lett.* **111**, 265701 (2013).
- <sup>124</sup>G. Li, I. Tamblyn, V. R. Cooper, H.-J. Gao, and J. B. Neaton, *Phys. Rev. B* **85**, 121409(R) (2012).
- <sup>125</sup>G. Li, T. Rangel, Z.-F. Liu, V. R. Cooper, and J. B. Neaton, *Phys. Rev. B* **93**, 125429 (2016).
- <sup>126</sup>L. Romaner, G. Heimel, C. Ambrosch-Draxl, and E. Zojer, *Adv. Func. Mater.* **18**, 3999 (2008).
- <sup>127</sup>A. Natan, N. Kuritz, and L. Kronik, *Adv. Func. Mater.* **20**, 2077 (2010).
- <sup>128</sup>S. Sharifzadeh, A. Biller, L. Kronik, and J. B. Neaton, *Phys. Rev. B* **85**, 125307 (2012).
- <sup>129</sup>D. Vanzo, B. J. Topham, and Z. G. Soos, *Adv. Func. Mater.* **25**, 2004 (2015).
- <sup>130</sup>S. C. Lam and R. J. Needs, *J. Phys.: Condens. Matter* **5**, 2101 (1993).
- <sup>131</sup>A. Bashir, D. Käfer, J. Müller, C. Wöll, A. Terfort, and G. Witte, *Angew. Chem., Int. Ed.* **47**, 5250 (2008).
- <sup>132</sup>N. Sato, K. Seki, and H. Inokuchi, *J. Chem. Soc., Faraday Trans. 2* **77**, 1621 (1981).
- <sup>133</sup>In the GW calculations, 1500 bands and an energy cutoff of 10 Ry are used to calculate the polarizability. The dielectric function is calculated using the generalized plasmon pole model. A box truncation and a single q-point ( $\Gamma$ ) are used for the molecule. A slab truncation and a  $8 \times 4 \times 1$  q-mesh are used for the monolayer. Static remainder is used in the evaluation of self-energy correction.

- <sup>134</sup>J. Deslippe, G. Samsonidze, D. A. Strubbe, M. Jain, M. L. Cohen, and S. G. Louie, *Computer Phys. Commun.* **183**, 1269 (2012).
- <sup>135</sup>Y. Zou, L. Kilian, A. Schöll, T. Schmidt, R. Fink, and E. Umbach, *Surf. Sci.* **600**, 1240 (2006).
- <sup>136</sup>A. Kraft, R. Temirov, S. K. M. Henze, S. Soubatch, M. Rohlfing, and F. S. Tautz, *Phys. Rev. B* **74**, 041402 (2006).
- <sup>137</sup>M. Rohlfing, R. Temirov, and F. S. Tautz, *Phys. Rev. B* **76**, 115421 (2007).
- <sup>138</sup>J. Ziroff, F. Forster, A. Schöll, P. Puschnig, and F. Reinert, *Phys. Rev. Lett.* **104**, 233004 (2010).
- <sup>139</sup>B. Stadtmüller, D. Lüftner, M. Willenbockel, E. M. Reinisch, T. Sueyoshi, G. Koller, S. Soubatch, M. G. Ramsey, P. Puschnig, F. S. Tautz, and C. Kumpf, *Nat. Commun.* **5**, 3685 (2014).
- <sup>140</sup>A. Bendounan, F. Forster, A. Schöll, D. Batchelor, J. Ziroff, E. Umbach, and F. Reinert, *Surf. Sci.* **601**, 4013 (2007).
- <sup>141</sup>A. Schöll, L. Kilian, Y. Zou, J. Ziroff, S. Hame, F. Reinert, E. Umbach, and R. H. Fink, *Science* **329**, 303 (2010).
- <sup>142</sup>J. Ziroff, S. Hame, M. Kochler, A. Bendounan, A. Schöll, and F. Reinert, *Phys. Rev. B* **85**, 161404(R) (2012).
- <sup>143</sup>T. Körzdörfer and S. Kümmel, *Phys. Rev. B* **82**, 155206 (2010).
- <sup>144</sup>W. Kohn, *Phys. Rev. Lett.* **76**, 3168 (1996).
- <sup>145</sup>N. Dori, M. Menon, L. Kilian, M. Sokolowski, L. Kronik, and E. Umbach, *Phys. Rev. B* **73**, 195208 (2006).
- <sup>146</sup>F. Rissner, D. A. Egger, A. Natan, T. Körzdörfer, S. Kümmel, L. Kronik, and E. Zojer, *J. Am. Chem. Soc.* **133**, 18634 (2011).
- <sup>147</sup>P. Puschnig, E.-M. Reinisch, T. Ules, G. Koller, S. Soubatch, M. Ostler, L. Romaner, F. S. Tautz, C. Ambrosch-Draxl, and M. G. Ramsey, *Phys. Rev. B* **84**, 235427 (2011).
- <sup>148</sup>G. D. Mahan, *Many-Particle Physics*, 3rd ed. (Springer, 2000).
- <sup>149</sup>J. Paier, M. Marsman, and G. Kresse, *J. Chem. Phys.* **127**, 024103 (2007).
- <sup>150</sup>T. Ules, D. Lüftner, E. M. Reinisch, G. Koller, P. Puschnig, and M. G. Ramsey, *Phys. Rev. B* **90**, 155430 (2014).
- <sup>151</sup>J. Jaramillo, G. E. Scuseria, and M. Ernzerhof, *J. Chem. Phys.* **118**, 1068 (2003).
- <sup>152</sup>M. A. L. Marques, J. Vidal, M. J. T. Oliveira, L. Reining, and S. Botti, *Phys. Rev. B* **83**, 035119 (2011).
- <sup>153</sup>L. Lin, *J. Chem. Theory Comput.* **12**, 2242 (2016).